Title

Measuring Diffusion of Lipid-like Probes in Artificial and Natural Membranes by Raster Image Correlation Spectroscopy (RICS): Use of a Commercial Laser-Scanning Microscope with Analog Detection

Journal

Langmuir, 25(9)

ISSN

0743-7463

Authors

Gielen, Ellen
Smisdom, Nick
vandeVen, Martin
et al.

Publication Date

2009-05-05

DOI

10.1021/la8040538

Langmuir
Article
pubs.acs.org/Langmuir

Measuring Diffusion of Lipid-like Probes in Artificial and Natural Membranes by Raster Image Correlation Spectroscopy (RICS): Use of a Commercial Laser-Scanning Microscope with Analog Detection

Ellen Gielen,[†,‡,⊥] Nick Smisdom,[†,⊥] Martin vandeVen,[†] Ben De Clercq,[†] Enrico Gratton,[§] Michelle Digman,[§] Jean-Michel Rigo,[†] Johan Hofkens,[∥] Yves Engelborghs,[‡] and Marcel Ameloot*[,†]

[†]*Laboratory for Cell Physiology, Biomedical Research Institute, Hasselt University and transnationale Universiteit Limburg, Agoralaan, Bldg C, B-3590 Diepenbeek, Belgium,* [‡]*Laboratory for Biomolecular Dynamics, Katholieke Universiteit Leuven, Celestijnenlaan 200G, B-3001 Heverlee, Belgium,* [§]*Laboratory for Fluorescence Dynamics, University of California, Biomedical Engineering Department, 3120 Natural Sciences 2, Irvine, California 92697-2715, USA and* [∥]*Laboratory for Photochemistry and Spectroscopy, Katholieke Universiteit Leuven, Celestijnenlaan 200F, 3001 Heverlee, Belgium.* [⊥]*Ellen Gielen and Nick Smisdom contributed equally to this work.*

Received December 9, 2008. Revised Manuscript Received February 4, 2009

The heterogeneity in composition and interaction within the cellular membrane translates into a wide range of diffusion coefficients of its constituents. Therefore, several complementary microfluorimetric techniques such as fluorescence correlation spectroscopy (FCS), fluorescence recovery after photobleaching (FRAP) and single-particle tracking (SPT) have to be applied to explore the dynamics of membrane components. The recently introduced raster image correlation spectroscopy (RICS) offers a much wider dynamic range than each of these methods separately and allows for spatial mapping of the dynamic properties. RICS is implemented on a confocal laser-scanning microscope (CLSM), and the wide dynamic range is achieved by exploiting the inherent time information carried by the scanning laser beam in the generation of the confocal images. The original introduction of RICS used two-photon excitation and photon counting detection. However, most CLSM systems are based on one-photon excitation with analog detection. Here we report on the performance of such a commercial CLSM (Zeiss LSM 510 META) in the study of the diffusion of the fluorescent lipid analog 1,1′-dioctadecyl-3,3,3′,3′-tetramethyl-indodicarbocyanine perchlorate (DiI-C_{18}(5)) both in giant unilamellar vesicles and in the plasma membrane of living oligodendrocytes, i.e., the myelin-producing cells of the central nervous system. It is shown that RICS on a commercial CLSM with analog detection allows for reliable results in the study of membrane diffusion by removal of unwanted correlations introduced by the analog detection system. The results obtained compare well with those collected by FRAP and FCS.

Introduction

A variety of complementary microfluorimetric methods is used to study the dynamics of membrane components in the exploration of the lateral heterogeneity of cellular membranes. These techniques comprise fluorescence recovery after photobleaching (FRAP), fluorescence correlation spectroscopy (FCS), single-particle tracking (SPT) and image correlation based methods.[1−10] Several of these techniques have been implemented on a confocal laser-scanning microscope (CLSM) allowing for substantial reduction of the signal contribution from planes out of focus.

Each technique has its specific dynamic range and characteristic merits. In the FRAP method, a brief intense excitation period is used to irreversibly photobleach fluorophores in a small area of the membrane. By monitoring the fluorescence recovery with time, the diffusion coefficient and the mobile fraction can be determined.[1,10] In FCS, small fluctuations in the fluorescence signal from a femtoliter observation volume are measured over a short period of time.[11,12] These fluctuations arise from fluorescently labeled molecules diffusing in and out of the observation volume. The corresponding autocorrelation function (ACF) contains information about the average number of molecules in the observation volume and their characteristic diffusion time.[13] Stationary FCS is limited to fast dynamical processes (microsecond-to-millisecond

*Corresponding author. Address: Hasselt University, Biomedical Research Institute, Laboratory of Cell Physiology, Agoralaan, Bldg C, B-3590 Diepenbeek, Belgium. Tel: 00-32-11-26.92.33. Fax: 00-32-11-26.92.99. E-mail: marcel.ameloot@uhasselt.be.

(1) Kenworthy, A. K.; Nichols, B. J.; Remmert, C. L.; Hendrix, G. M.; Kumar, M.; Zimmerberg, J.; Lippincott-Schwartz, J. *J. Cell. Biol.* **2004**, *165*, 735– 746.
(2) Schwille, P.; Korlach, J.; Webb, W. W. *Cytometry* **1999**, *36*, 176–182.
(3) Bacia, K.; Scherfeld, D.; Kahya, N.; Schwille, P. *Biophys. J.* **2004**, *87*, 1034–1043.
(4) Srivastava, M.; Petersen, N. O. *Biophys. Chem.* **1998**, *75*, 201–211.
(5) Wiseman, P. W.; Squier, J. A.; Ellisman, M. H.; Wilson, K. R. *J. Microsc.* **2000**, *200*, 14–25.
(6) Petersen, N. O. *Fluorescence Correlation Spectroscopy: Theory and Applications*; Springer: New York, **2001**; Chapter 8.
(7) Costantino, S.; Comeau, J. W.; Kolin, D. L. *Biophys. J.* **2005**, *89*, 1251–1260.
(8) Dietrich, C; Yang, B; Fujiwara, T; Kusumi, A; Jacobson, K. *Biophys. J.* **2002**, *82*, 274–84.
(9) Lenne, P. F.; Wawrezinieck, L.; Conchonaud, F.; Wurtz, O.; Boned, A.; Guo, X. J.; Rigneault, H.; He, H. T.; Marguet, D. *EMBO J.* **2006**, *25*, 3245–3256.
(10) Marguet, D.; Lenne, P. F.; Rigneault, H.; He, H. T. *EMBO J.* **2006**, *25*, 3446–3457.
(11) Rigler, R.; Elson, E. S. *Fluorescence Correlation Spectroscopy: Theory and Applications*; Springer: New York, **2001**.
(12) Bacia, K.; Schwille, P. *Methods* **2003**, *29*, 74–85.
(13) Haustein, E.; Schwille, P. *Curr. Opin. Struct. Biol.* **2004**, *14*, 531–540.

time scale) occurring at a single fixed spot within the cell membrane. The recently introduced raster image correlation spectroscopy (RICS; Digman et al.[14,15]) allows exploration of molecular mobility over a wide dynamic range by exploiting the inherent time information associated with the scanning laser beam. Adjacent pixels along a single (horizontal) line are a few to several hundred microseconds (pixel dwell time) apart, while pixels over successive (vertical) lines and frames are, respectively, a few milliseconds (line scan time) and seconds-to-minutes apart. An additional advantage of RICS is that kinetic information can be spatially mapped, allowing for the detection of heterogeneities in diffusion.[14−16]

The original introduction of RICS made use of two-photon excitation and photon counting detection and was applied to measure diffusion in the three-dimensional (3D) space.[14,15] Very recently the implementation of RICS on a commercial CLSM with one-photon excitation and analog detection was described to measure protein diffusion in three[16] and two[17] dimensions.

In this report, our earlier investigations[17] concerning the determination and the spatial mapping of diffusion coefficients in membranes by RICS implemented on a standard CLSM with one-photon excitation and analog detection is extended. Control measurements on subresolution fluorescent beads in isotropic viscous solution were performed to validate the method. The applicability of RICS to monitor two-dimensional (2D) diffusion was evaluated in a well-defined system consisting of 1-palmitoyl-2-oleoyl-*sn*-glycero-3-phosphatidylcholine (POPC) giant unilamellar vesicles (GUVs) containing the lipid probe 1,1′-dioctadecyl-3,3,3′,3′-tetramethyl-indodicarbocyanine perchlorate (DiI-C_{18}(5)). This system was also characterized by means of beam expander FCS.[9,18,19] Both RICS and FRAP were applied to monitor the diffusion of DiI-C_{18}(5) in the membrane of primary oligodendrocytes (OLGs) derived from neonatal rat brain.

Materials and Methods

Chemicals. Fluorescent latex beads (175 nm diameter, PS-Speck microscope point source kit, yellow-green, excitation λ = 505 nm/emission λ = 515 nm), 120 μm thick adhesive spacers (Secure-seal spacer), DiI-C_{18}(5), Alexa Fluor 633-C_5-maleimide, and Cy5 were purchased from Molecular Probes, Eugene, OR, supplied by Invitrogen, Merelbeke, Belgium. POPC was purchased from Avanti Polar Lipids, Alabaster, AL. Dulbecco's modified Eagle's medium (DMEM), penicillin, streptomycin and L-glutamine were bought from Gibco BRL (supplied by Invitrogen). Fetal bovine serum (FBS), poly-L-lysine (PLL), bovine serum albumin fraction V (BSA V), progesterone, putrescine, sodium selenite, triiodothyronine, thyroxine, insulin, and holo-transferrin were purchased from Sigma-Aldrich, Bornem, Belgium. Water was Milli-Q grade.

GUVs. GUVs with a diameter varying from 10 up to 100 μm were formed by electroformation.[20,21] A homemade closed bath chamber was equipped with two square glass coverslips (22 × 22 mm, 175 μm thick), each coated with optically transparent and electrically conductive indium tin oxide (ITO; Präzisions Glas & Optik GmbH, Iserlohn, Germany), and a 3 mm thick square silicone rubber spacer with an 18 mm inside diameter. A mixture of POPC and DiI-C_{18}(5) (lipid/dye 40 000:1) was formed in chloroform. A 2.5 μL portion of the lipid mixture was deposited on the bottom ITO glass by means of a Hamilton syringe. The solvent was dried in an oven at 50 °C (15 min), and, after the addition of water, an AC voltage of 1.5 V at 10 Hz was applied for 30 min at room temperature (RT). RICS and FRAP measurements were performed at the top membrane (i.e., facing the bathing solution) of the GUVs. A fluid phase was assured by performing the measurements at RT.

Primary OLG Cultures Derived from Neonatal Rat Brain. Primary mixed brain cell cultures were prepared from brains of 1−2-day-old Wistar rats (Harlan Netherlands B.V., Horst, The Netherlands). The rats were decapitated, their forebrains were collected, the meninges were removed, and the cells were dissociated mechanically by cutting the tissue in smaller pieces followed by successive passages through 18G, 21G, and 23G needles, respectively. Cells were collected by centrifugation (80 g for 5 min at RT; Eppendorf Centrifuge 5804R, VWR, Leuven, Belgium), and a single cell suspension was prepared by repeated pipetting through a 1 mL pipet. The cells were resuspended in culture medium containing DMEM (cat. no. 41965-039) supplemented with 10% FBS, 100 U/mL penicillin, 100 μg/mL streptomycin, and 2 mM L-glutamine and seeded at approximately 1.5 brain per 75 cm^2 flasks precoated with PLL (5 μg/mL for 1 h at RT). The culture medium was changed 4 days after seeding and twice a week thereafter. The oligodendrocyte progenitor cells (OPCs) appeared as round-shaped, phase-dark cells on top of a layer of astrocytes. After 10−14 days in culture, OPCs were collected by mechanical shaking (180 rpm for 1 h at 37 °C, medium change, 240 rpm for 18 h at 37 °C; Innova 4000 shaking incubator, New Brunswick Scientific NV-SA, Rotselaar, Belgium) as described by McCarthy and de Vellis,[22] followed by differential adhesion. Cells were seeded at 75 000 cells per 24 mm diameter PLL-coated (10 μg/mL for 45 min at RT) glass coverslip and cultured for 2 days in a defined SATO medium (DMEM (cat. no. 41965-039) supplemented with 100 U/mL penicillin, 100 μg/mL streptomycin, 2 mM L-glutamine, 100 μg/mL BSA V, 60 ng/mL progesterone, 16 μg/mL putrescine, 5 ng/mL sodium selenite, 400 ng/mL triiodothyronine, 400 ng/mL thyroxine, 5 μg/mL insulin, and 50 μg/mL holotransferrin) in the presence of 10 ng/mL platelet-derived growth factor (PDGFα) and 10 ng/mL fibroblast growth factor (FGF-2; Preprotech, Rock Hill, NJ, USA). OLG differentiation was induced by removal of the growth factors and by cultivating the cells in SATO medium containing 0.5% FBS. Immature myelinating cells[23] were labeled for 3 min at RT with 10 μM of the membrane marker DiI-C_{18}(5) for FRAP and RICS measurements. Excessive DiI-C_{18}(5) was removed by five washing steps with HEPES buffered medium without phenol red.

RICS: Principles. The principles of RICS are briefly reiterated here for reference purposes and the reader is referred to the original papers by Digman et al.[14,15] for more details. The transition from FCS to RICS is made by defining a scan function that relates time with space:

$$\tau(\xi, \psi) = \tau_p \xi + \tau_l \psi \quad (1)$$

(14) Digman, M. A.; Brown, C. M.; Sengupta, P.; Wiseman, P. W.; Horwitz, A. R.; Gratton, E. *Biophys. J.* **2005**, *89*, 1317–1327.
(15) Digman, M. A.; Sengupta, P.; Wiseman, P. W.; Brown, C. M.; Horwitz, A. R.; Gratton, E. *Biophys. J.* **2005**, *88*, L33–L36.
(16) Brown, C. M.; Dalal, R. B.; Hebert, B.; Digman, M. A.; Horwitz, A. R.; Gratton, E. *J. Microsc.* **2008**, *229*, 78–91.
(17) Gielen, E.; Smisdom, N.; De Clercq, B.; vandeVen, M.; Gijsbers, R.; Debyser, Z.; Rigo, J. M.; Hofkens, J.; Engelborghs, Y.; Ameloot, M. *J. Fluoresc.* **2008**, *18*, 813–819.
(18) Wawrezinieck, L.; Rigneault, H.; Marguet, D.; Lenne, P. F. *Biophys. J.* **2005**, *89*, 4029–4042.
(19) Wawrezinieck, L.; Lenne, P. F.; Marguet, D.; Rigneault, H. *Proc. SPIE Int. Soc. Opt. Eng.* **2004**, *5462*, 92–103.
(20) Angelova, M. I.; Dimitrov, D. *Faraday Discuss. Chem. Soc.* **1986**, *81*, 303–311.
(21) Angelova, M. I.; Soléau, S.; Meléard, P.; Faucon, J. F.; Bothorel, P. *Prog. Colloid Polym. Sci.* **1992**, *89*, 127–131.
(22) McCarthy, K. D.; de Vellis, J. *J. Cell. Biol.* **1980**, *85*, 890–902.
(23) Baumann, N.; Pham-Dinh, D. *Physiol. Rev.* **2001**, *81*, 871–927.

where τ_p and τ_l denote, respectively, pixel dwell time and line scan time, and where ξ and ψ refer to the spatial displacements in the x (pixels along a horizontal line) and y (pixels in successive lines) direction in the raster image. The overall normalized fluorescence intensity fluctuation spatial ACF ($G_S(\xi,\psi)$) is defined as

$$G_S(\xi,\psi) = \frac{\langle \delta I(x,y)\delta I(x+\xi, y+\psi)\rangle_{x,y}}{\langle I(x,y)\rangle_{x,y}^2} = G(\xi,\psi)S(\xi,\psi) \quad (2)$$

where $I(x,y)$ is the detected fluorescence intensity at each pixel and $\delta I(x,y) = I(x,y) - \langle I(x,y)\rangle_{xy}$ are the fluorescence intensity fluctuations around the mean intensity of the image $\langle I(x,y)\rangle_{xy}$. The ACF for 3D diffusion and for one-photon excitation is given by

$$G(\xi,\psi) = \frac{\gamma}{N}\left(1 + \frac{4D(\tau_p\xi + \tau_l\psi)}{\omega_0^2}\right)^{-1}\left(1 + \frac{4D(\tau_p\xi + \tau_l\psi)}{\omega_z^2}\right)^{-1/2} \quad (3)$$

with D the diffusion coefficient, N the average number of molecules in the volume of observation and ω_0 and ω_z, respectively, the lateral and axial waist of the laser beam at the point of focus. For diffusion in a plane the last factor in eq 3 must be omitted. The factor γ accounts for the nonuniform illumination of the excitation volume and is equal to 0.3535 for a 3D[24] and 0.5 for a 2D Gaussian point spread function (PSF).[25] $G(\xi,\psi)$ is the ACF due to molecular diffusion only. Since the PSF extends over several pixels in the xy-plane (requisite for RICS), the correlation due to the scanning itself has to be considered. For square pixels with dimension $\delta r \times \delta r$ this correlation ($S(\xi,\psi)$) is given by

$$S(\xi,\psi) = \exp\left(-\frac{\left[\left(\frac{\xi\delta r}{\omega_0}\right)^2 + \left(\frac{\psi\delta r}{\omega_0}\right)^2\right]}{1 + \frac{4D(\tau_p\xi+\tau_l\psi)}{\omega_0^2}}\right) \quad (4)$$

RICS: Instrumentation. Raster-scan images were collected with a Zeiss LSM 510 META one-photon CLSM (Jena, Germany, SN 002-11332, installed November 2002; scan parameter values appear to be dependent on the serial number) on an Axiovert200 M motorized frame placed on a vibration isolation table in an air-conditioned room kept at constant temperature. An analog photomultiplier tube (PMT; model is proprietary Zeiss information) was used for detection. Dark signal contributions to the images were effectively zeroed out by setting the proper detection offset value as provided in the Zeiss software. Fluorescent latex beads were excited with the 488 nm line (selected by an extra 488 ± 10 nm interference-based laser cleanup filter) of the 30 mW air-cooled argon ion laser under the control of an acousto-optical tunable filter (AOTF; set at 1% transmission; 10 μW at the sample position as measured with a Coherent LaserMate Q powermeter (Coherent B.V., Utrecht, The Netherlands)). The excitation light was directed to the sample by a dichroic mirror (DC; HFT 488) and a Zeiss EC Plan-Neofluar 40×/NA 1.3 oil immersion objective. The fluorescence light was sent through the DC and a long-pass LP505 emission filter to the PMT. POPC/DiI-C_{18}(5) GUVs and primary OLG membranes containing DiI-C_{18}(5) were excited with a 5 mW 633 nm He−Ne laser (set at 1% of the AOTF transmission). The excitation light was reflected by a DC (HFT UV/488/543/633) and focused onto the sample through the EC Plan-Neofluar 40×/NA 1.3 oil immersion objective. The fluorescence emission was sent through the DC, and a bandpass BP650-710 emission filter to the PMT. During collection of the image series, the membrane stayed in focus, and the setup was thermally stable. Out-of-plane fluorescence was reduced by a pinhole (1 airy unit, i.e., 66 and 90 μm for the green and red channels, respectively) in front of the detector. Images were collected using the Zeiss system control software version 4.0 SP2. The image size was typically set to 512 × 512 pixels, and the zoom factor was set to 8 (54.9 nm/pixel) to ensure that the PSF contained a sufficiently large number of pixels (radius of 5−6 pixels). The detector gain was set to 900 Zeiss software units. The $1/e^2$ axial and lateral waists of the PSF were determined by performing a z-stack on 175 nm immobilized fluorescent beads, followed by applying the point distiller and data processing Huygens Essential software package (Scientific Volume Imaging, Hilversum, The Netherlands). The obtained intensity profiles in the xy-direction and in the z-direction were subsequently fit with a Gaussian profile using Origin (OriginLab Corp, Northampton, MA, USA) or Matlab (Matlab R2007b version 7.4, The MathWorks BV, Eindhoven, The Netherlands).

RICS: Correlated Detector Noise. The integration circuit in analog detectors can introduce unwanted correlations. A fast Fourier transform (FFT) of the raw images as well as inspection of the ACFs showed that the collected dark current images (i.e., the laser is switched off) only exhibited an influence of correlated noise in the x-axis scan direction. No correlated noise was observed in the y-scan direction. The latter noise component typically would show up as a periodic sinewave signal due to, for example, vibrational coupling of the microscope stage to running cooling fans. Contrary to the systems with analog detection electronics as described by Brown,[16] who reported at most a few pixels in the x-scan $\psi = 0$ direction with correlated noise, our LSM 510 META consistently showed substantially more pixels with correlated noise along the x-axis. For PMT gain settings of 600−1100 (Zeiss software units) and various scan speeds, 15−30 pixels along the $\psi = 0$ x-axis scan direction have to be discarded. This was checked by looking at the correlation spectrum of dark current images collected at various scan speeds (1−13, corresponding to pixel dwell times ranging from 163.84 to 0.57 μs). These pixel dwell time values may vary according to the series number of a particular confocal instrument. As shown in Figure 1, all data points in the $\xi-\psi$ plane are close to zero aside from the central $G(0,0)$ noise peak. The width of this peak depends on the pixel dwell time τ_p and the characteristic correlation time of the PMT and associated electronics (i.e., ≈ 5.7 μs for our setup). For short pixel dwell times (i.e., fast scanning), the noise peak spreads out over many pixels, because the characteristic correlation time is several times larger than the respective τ_p. Note, as mentioned above, that the detection noise only correlates in the ξ-direction (i.e., along the horizontal line scan direction) and not in the ψ-direction, among others because the line scan time is orders of magnitude larger than the detector correlation time. Practically, in the analyses discussed below, the $\psi = 0$ line was not taken into account.

(24) Müller, B. K.; Zaychikov, E.; Brauchle, C.; Lamb, D. C. *Biophys. J.* **2005**, *89*, 3508–3522.
(25) Thompson, N. Fluorescence correlation spectroscopy. *Topics in Fluorescence Spectroscopy*; Plenum: New York, **1991**; pp 333−378.

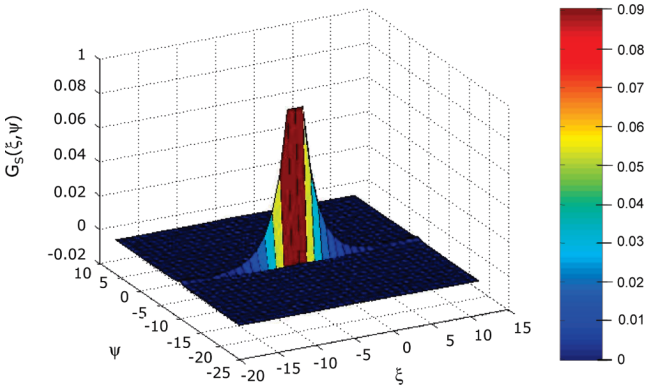

Figure 1. Correlation spectrum (truncated along the $G_S(\xi,\psi)$ axis for display purposes) showing the noise peak generated by the PMT. Scales for the ξ and ψ axes are in pixels. 100 dark current images were collected at a scan speed of 13 ($\tau_p = 0.57\,\mu s$; $\tau_l = 0.684$ ms; $T = 23$ °C, detector gain = 900 Zeiss software units). Color bar maps $G_S(\xi,\psi)$ values.

RICS: Data Analysis Software. The group at Hasselt University separately developed a RICS data analysis program (UH RICS program) within the Matlab environment, incorporating routines as made available by D.L. Kolin (McGill University, Montreal, Quebec, Canada) and described by Costantino et al.[7] To corroborate the results, data were also analyzed with the original RICS software (UCI RICS program) from the Laboratory for Fluorescence Dynamics (E. Gratton, University of California, Irvine, CA). Simulations with the possibility to add noise were run with the UH RICS program to determine the optimal scan speed for recovery of the diffusion coefficient. The parameters of the models were estimated by weighted nonlinear least-squares, with weights calculated from the standard errors (σ) of the set of ACFs determined from the images of the series. In practice, it is advised to include in the fitting procedure only the data in the correlation spectrum to about 3 times the width of the laser beam at its focal point.[26] Since raster-scan images have a finite size, there is less information available at long lag distances to calculate the correlation function. As a result, the spatial correlation functions do not always decay to zero. It is therefore advisable to include a constant offset in the fit functions.[25] Before performing the correlation analyses, one should filter out large immobile structures from the images since they will appear as strong long-range spatial correlations in the autocorrelation spectrum and hide other potentially more meaningful information.[14−16] This can be done by applying an immobile fraction removal algorithm.[14−16] The correlation spectrum then only contains information about the moving particles. This overall immobile fraction removal algorithm was applied to correct for the background (assuming that the background can be considered as an immobile fraction) in the case of fluorescent beads and POPC/DiI-C_{18}(5) GUVs. In the case of cell measurements, however, both the cell itself as well as its subcellular structures may slowly move during image acquisition. Applying the overall immobile fraction removal algorithm will in this case result in a broadening of the spatial ACF since the movements prevent complete removal of the "immobile" structures.[16] Rather, a short-range moving average immobile removal algorithm should be used. In this study, a moving average window of two frames was applied to all image stacks collected in cells before calculation of the autocorrelation spectra.

RICS: Image Noise and Mapping Reliability Simulations. Images collected for 2D free translational diffusion in GUV and cell membranes contain, apart from the fluorescence from the incorporated fluorophores, a background fluorescence signal and detector dark signal. In analog detection signals, both uncorrelated and amplifier electronics-related multiplicative correlated noise components are present. As mentioned earlier, it is found that correlated noise was only present in the x-axis scan direction in the one-photon LSM 510 META images, and its extent in the ACFs depends on the PMT gain and scan parameter settings. Our particular analog detection system shows a strong noise presence along the $\psi = 0$ line for well over 15 pixels. Nonetheless, for certain gain and scanspeed settings, a usable combination exists. Choosing detection gain settings below 1000 (Zeiss software units) and for scanspeeds 1 and 2 with long pixel dwell times $\tau_p = 163.84$ and 102.4 μs, respectively, the dark image ACF $G(\xi,\psi)$ values appear to be essentially random and very small around the $\psi = 0$ line for all pixels. For all other setting combinations, this was not the case. Therefore, the $\psi = 0$ line had to be discarded for the diffusion times encountered. In these cases, the dynamic range can be estimated to be completely dependent on the line time. Since this x-axis component did not have to be considered in the actual analyses, only the influence of uncorrelated noise in the slow y-axis scan direction was explored. 2D membrane-like free translational diffusion simulations without (UCI simFCS and RICS and UH RICS) and with (UH RICS) varying degrees of counting noise were carried out to estimate its influence on the retrieved D mapping values. Collected at nonsaturating PMT gain settings of 600−1100 (Zeiss software settings), low-intensity GUV images showed a Poissonian intensity histogram, while the brighter cell images showed histograms well approximated by a Gaussian distribution. The simulation of these images was analogous to that of Costantino[7] and Kolin[27] with planar 2D membrane free diffusion point sources representing large aggregates or transmembrane proteins with $D = 0.1\,\mu m^2/s$ or lipids and probes in membranes with $D = 5\,\mu m^2/s$.[16]

For comparison, all simulation parameters were kept as close as possible to the experimental settings: Stacks of 100 images were generated each 256 × 256 pixels wide, with 54.9 nm/pixel (50 nm/pixel for UCI RICS simulations). Radial and axial PSF values were respectively 260 and 890 nm (40x/NA 1.3 oil objective, zoom 8) as determined with a Gaussian fit to averaged Z-scan images of subresolution beads. The accuracy of these fits was typically 2% ($n = 9$, where n is number of repeats). Pixel dwell times as obtained from a calibration of the actually present LSM 510 scan parameter values were 163.84 μs for $D = 0.1\,\mu m^2/s$ and 6.4 μs for $D = 5\,\mu m^2/s$. Varying degrees of counting noise (0.1, 1, 10, 100%) were added. The total particle number in a single image was set at 100, 500 and 2500. For a 32 × 32 pixel analysis region (1.76 × 1.76 μm^2) in a single image, this respectively corresponds to 1.56, 7.8, and 39 particles in the observation volume. Continuous boundary conditions were used. Simulations typically took from several tens of minutes to hours on a 3 GHz dual core computer.

(26) Petersen, N. O. *Fluorescence Correlation Spectroscopy: Theory and Applications*; Springer: New York, **2001**; Chapter 8.

(27) Kolin, D. L.; Costantino, S.; Wiseman, P. W. *Biophys. J.* **2006**, *90*, 628–639.

Using an ACF cropping size of 3 times the ACF width,[26] the simulated sets of 100 images were mapped for decreasing analysis region of interest (ROI) sizes of 256 × 256, 128 × 128, 64 × 64 and 32 × 32 pixels, corresponding to regions extending from 14 × 14 down to 1.76 × 1.76 μm^2. Results were normalized to those for the initial image size of 256 × 256 pixels. Figure 2 corroborates the work of Brown[16] in that, by decreasing the size of the analysis ROI, the ACF becomes noisier and less well-defined, resulting in a drop in retrieved D values due to undersampling. When simulations for a total number of particles of $N = 100$ are analyzed for a reduced set of just 15 images, ill-defined noisy ACFs result for 128 × 128 and smaller size analysis mapping ROIs with ill-retrieved D values due to a lack of particles in these small analysis mapping bricks.

Figure 2 shows that, similar to that found by Brown,[16] there is a drop off in retrieved D values of about 30% for $D = 0.1\ \mu$m^2/s. Errors bars for small analysis ROIs decrease when more particles are present in the illuminated volume. Analysis results for small brick size with a total number of particles N equal to 2500 slightly better resemble the input value. A sufficient number of images and particles have to be present. As mentioned, using a subset of just 15 images for $D = 0.1\ \mu$m^2/s and a small total number of particles $N = 100$ gave an almost 90% reduction in the retrieved D value. The addition of even large amounts of random uncorrelated counting noise did not influence the simulation results significantly. From these results it is to be expected that 32 × 32 pixel mapping analysis (1.76 μm × 1.76 μm for 40× oil objective, zoom 8 conditions) of particular well-selected areas with apparent homogeneous fluorescence intensity in a cell membrane image stack will give reproducible values. We purposely added a significant amount of counting noise over and above the real signal histograms, but, since this added signal is uncorrelated, the ACF is rather well retrieved.

The smaller the D values simulated, the more sensitive the analysis becomes for proper scanspeed selection due to an ever more circular and less elliptical shape of the ACF. A value for D equal to 20 μm^2/s (data not shown) has a very elliptical ACF, which consistently is easily retrieved.

FCS. Standard FCS measurements are performed at a single size of the observation volume. Wawrezinieck et al.[18] introduced the "FCS diffusion law" concept, which requires the collection of ACFs at different sizes of the excitation laser beam. For hindered or confined diffusion, and for the case where the area of confinement is several times smaller than the beam area, the relation between the diffusion time, τ_d, and the beam area (i.e., the so-called "FCS diffusion law") can be described by

$$\tau_d = t_0 + \frac{\omega^2}{4D_{eff}} \tag{5}$$

where ω is the radius of the beam at the plane of diffusion, D_{eff} is the so-called effective diffusion coefficient, and t_0 is a constant.[18] For free diffusion, t_0 is equal to zero. A nonzero value for t_0 in the FCS diffusion law is indicative of hindered diffusion. If $t_0 > 0$, the confinement is due to dynamic partitioning in "rafts". If $t_0 < 0$, the confinement is due to interaction with the cytoskeleton meshwork.[9,18] These measurements at different waist sizes

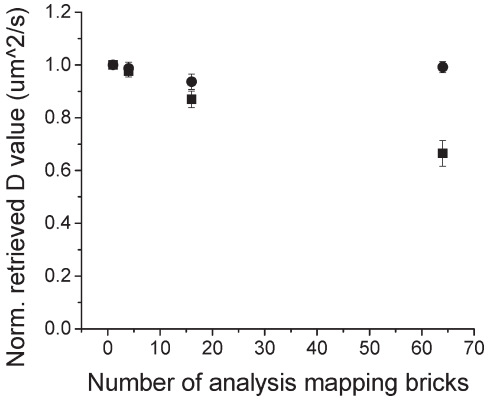

Figure 2. Simulation results for a set of 100 256 × 256 images containing a total number of particles of 500 for various analysis mapping brick ROI sizes. Modeling parameter values for a free translational membrane diffusion $D = 0.1\ \mu$m^2/s with a pixel dwell time of $\tau_p = 163.84\ \mu$s (■) and $D = 5\ \mu$m^2/s with pixel dwell time $\tau_p = 6.4\ \mu$s (•). Retrieved D values are normalized to the D value obtained for the 256 × 256 input frame size. Error bars reflect standard error of the mean of the retrieved D values for the mapping ROIs.

can be accomplished by using a beam expander and an iris diaphragm.[19,28]

Beam expander FCS measurements, in which the diameter of the laser beam was adapted by means of a diaphragm, were performed on an IX70 Olympus (Olympus Belgium N. V., Aartselaar, Belgium) microscope equipped with a 5 mW 633 nm He−Ne laser (model HRT050, Thorlabs GmbH, Dachau/Munich, Germany). The excitation light was directed to the back aperture of an Olympus Plan-Apo 40x/NA 0.9 water immersion objective via a 620/40 nm BP excitation filter, a telescopic system with two lenses, a diaphragm, a Berek retardation compensator, two neutral density filters, a set of mirrors and a LP660 DC. The fluorescence emission was directed to the avalanche photodiode (APD; SPCM-AQR-14, PerkinElmer, N.V./S.A., Zaventem, Belgium) via two emission filters (LP660 and LP655). The detection pinhole was set at 50 μm. In this type of measurement, the radius of the beam at the plane of diffusion corresponds with ω_0, the radius of the beam at the waist. Two independent GUV samples were prepared and, for each of them, data from at least eight different GUVs were recorded with five repeat traces, each with 15 s acquisition time, per beam diameter (five different waists). The ALV-5000/EPP hardware correlator (ALV-GmbH, Langen, Germany) constantly recalculated the normalized ACFs during the measurement. All ACFs were fitted with a model considering 2D diffusion of a single species and, in addition to its triplet formation, taking possible *cis*−*trans* transitions of DiI-C_{18}(5) into account (2D2Tr1P):

$$G(\tau)_{2D} = 1 + \frac{\gamma}{N}\frac{1}{1 + \left(\frac{\tau}{\tau_d}\right)}\left[1 + \sum_{i=1}^{2}\frac{T_i}{1 - T_1 - T_2}\exp\left(-\frac{\tau}{\tau_{0i}}\right)\right] \tag{6}$$

where τ_{01} and τ_{02} are the inverse of the triplet rate constant and the *cis*−*trans* transition rate constant, respectively, and T_1 and T_2 are the corresponding amplitude fractions. The dimensions of the five different observation volumes

(28) Masuda, A.; Ushida, K.; Okamoto, T. *Biophys. J.* **2005**, *88*, 3584–3591.

were deduced from calibration measurements on Alexa Fluor 633-C_5-maleimide (D = 198 $\mu m^2/s$) [29−31] diffusing freely in water.

FRAP. The excitation light of the 5 mW 633 nm He−Ne laser of the Zeiss LSM 510 META one-photon CLSM (Jena, Germany) was reflected by a DC (HFT UV/488/543/633) and focused onto the sample through the Plan-Neofluar 40x/NA 1.3 oil immersion objective. The fluorescence emission was sent through the DC and a BP 650−710 emission filter to the PMT. Out-of-plane fluorescence was reduced as much as possible by setting the detection pinhole to 1 airy unit (90 μm diameter), which, under these conditions corresponds to an optical slice thickness of <1.2 μm. For measurements in primary OLGs, the stage position and focus were moved in order to have the ROI centered underneath the nucleus on the membrane facing the glass coverslip. In the case of GUVs, FRAP measurements were performed on the top membrane facing the bathing solution. The zoom factor was set to 8, the PMT gain and signal amplification were adapted in order to have a sufficiently high signal without any saturated pixels, and all measurements were performed at RT. Each FRAP experiment contains 70 images: 5 prebleach and 65 postbleach images. All images were collected at 1% of the AOTF transmission to prevent acquisition bleach as much as possible. The diameter of the circular ROIs for bleaching varied between 50 and 206 pixels (2.745 μm − 11.309 μm). The bleaching was performed by a single scan of the ROI with the AOTF transmission set to 30−100%. A sufficiently short bleach time and a ratio 1/4 between the frame time and τ_d were obtained by adapting the image size, the scan speed and the delay time. It is worthwhile to mention that these criteria were not fulfilled in the case of the GUVs, where only small ROIs could be analyzed because of the small top membrane area well in focus. The small ROIs, however, were not used for determination of D, but rather to quantify the mobile fraction of DiI-C_{18}(5). Since the curvature of the membrane of the GUVs prevented the use of a control region, the readout bleaching was corrected using an exponential function. In case of the primary OLGs, the whole cell surface at a sufficient distance from the bleach ROI was used to correct for readout bleaching. FRAP curves were fit as described by Soumpasis.[32]

Viscosity Determination. The viscosities of HEPES containing 5% Tween 20, and 2−56% sucrose in HEPES were determined with a model AR G-2 rheometer (Tain Instruments Corp., division of Waters NV/SA, Zellik, Belgium) at 23 °C. The instrument was calibrated before every measurement, and care was taken to avoid the introduction of air bubbles or the presence of air drafts. Each sample (1 mL, filtered through a 0.22 μm Sterivex filter, Millipore Corporation, supplied by VWR International Europe BVBA, Leuven, Belgium) was allowed to equilibrate for at least 10 min before measurements were started.

Results

RICS Validation: 3D Diffusion Measurements in Isotropic Solution. The RICS method was evaluated by performing measurements on 175 nm diameter green fluorescent beads freely diffusing in isotropic solutions of different viscosities (0−56% (w/v) sucrose in 20 mM HEPES pH 7.2) at 23 °C. To perform RICS measurements, the fluorescent beads were "sandwiched" between a microscope slide and a coverslip, sealed by an adhesive spacer. The resulting microscopic chamber is small enough to eliminate any flow in the solution while retaining a 3D sample environment.[33] Raster-scan images were collected at various scan speeds ranging from a scan speed of 2 (τ_p = 102.4 μs; τ_l = 122.88 ms) up to a scan speed of 13 (τ_p = 0.57 μs; τ_l = 0.68 ms). Before performing the correlation analyses, the respective backgrounds were subtracted by applying an overall immobile fraction removal algorithm. Autocorrelation spectra were cropped to 32 × 32 regions and fitted with a 3D free diffusion model. The results obtained by either analysis program were essentially independent of the initial guesses of the parameter values. For the results shown in Figure 3, a 256 × 256 ROI, the upper left quadrant of the collected 512 × 512 pixel images was selected for data analysis. As summarized in Table 1, the measured and expected D values according to the Stokes−Einstein equation are well in agreement. For each combination of solute and solvent, the diffusion coefficient was found to be essentially independent of the selected values of τ_p and τ_l within the range indicated above.

FCS on DiI-C_{18}(5) in POPC GUVs. Diaphragm FCS measurements were performed on eight different GUVs of the same sample, resulting in forty ACFs per diaphragm opening (data not shown). All ACFs per diaphragm diameter were pooled in a single analysis. The FCS diffusion law (eq 5) intercepts the time axis at the origin at almost zero t_0 value (t_0 = −0.07 ± 0.01 ms). The D_{eff} values, calculated from the slope of the separate plots (data not shown), vary from D_{eff} = 6.65 ± 0.06 $\mu m^2/s$ to D_{eff} = 9.9 ± 0.3 $\mu m^2/s$ (weighted average: D_{eff} = 7.64 ± 0.03 $\mu m^2/s$). The slope of the average FCS diffusion law yields a D_{eff} = 7.88 ± 0.03 $\mu m^2/s$. The effective diffusion coefficient becomes D_{eff} = 8.02 ± 0.01 $\mu m^2/s$ when t_0 is fixed at zero.

FRAP Measurements on DiI-C_{18}(5) in POPC GUVs. The diffusive motion of DiI-C_{18}(5) was too fast to allow for accurate determination of the diffusion time on the confocal setup. However, the mobile fraction, M, of DiI-C_{18}(5) was assessed in terms of the percentage of fluorescent molecules recovered in the bleached area during FRAP experiments. Measurements were performed at the top membrane of six individual GUVs. The weighted mean M value for DiI-C_{18}(5) is M = 97 ± 2%.

RICS Measurements on DiI-C_{18}(5) in POPC GUVs. Like FCS and FRAP measurements, RICS experiments were performed at the top membrane facing the bathing solution. RICS measurements were carried out on nine GUVs from two separate sample preparations. A typical image of the top membrane of a GUV is shown in Figure 4 together with the corresponding spatial ACF. After subtraction of the background by means of an overall immobile removal algorithm, in each GUV a 128 × 128 ROI was chosen in the middle of the top membrane for data analysis (Figure 4A). The resulting autocorrelation spectrum was cropped to a 32 × 32 pixels region and fitted with a 2D free diffusion model. The mean D value is D = 7 ± 3 $\mu m^2/s$. By analyzing in detail the GUV data with increasingly large GUV-centered ROIs in size ranging from 32 × 32 via 64 × 64 to 128 × 128 pixels, very

(29) Hutschenreiter, S.; Tinazli, A.; Model, K.; Tampe, R. *EMBO J.* **2004**, *23*, 2488–2497.
(30) van den Bogaart, G.; Krasnikov, V.; Poolman, B. *Biophys. J.* **2007**, *92*, 1233–1240.
(31) Sheng, N-S. *Ind. Eng. Chem. Res.* **2008**, *47*(9), 3285–3288.
(32) Soumpasis, D. M. *Biophys. J.* **1983**, *41*, 95–97.
(33) Braeckmans, K.; Remaut, K.; Vandenbroucke, R. E.; Lucas, B.; De Smedt, S. C.; Demeester, J. *Biophys. J.* **2007**, *92*, 2172–2183.

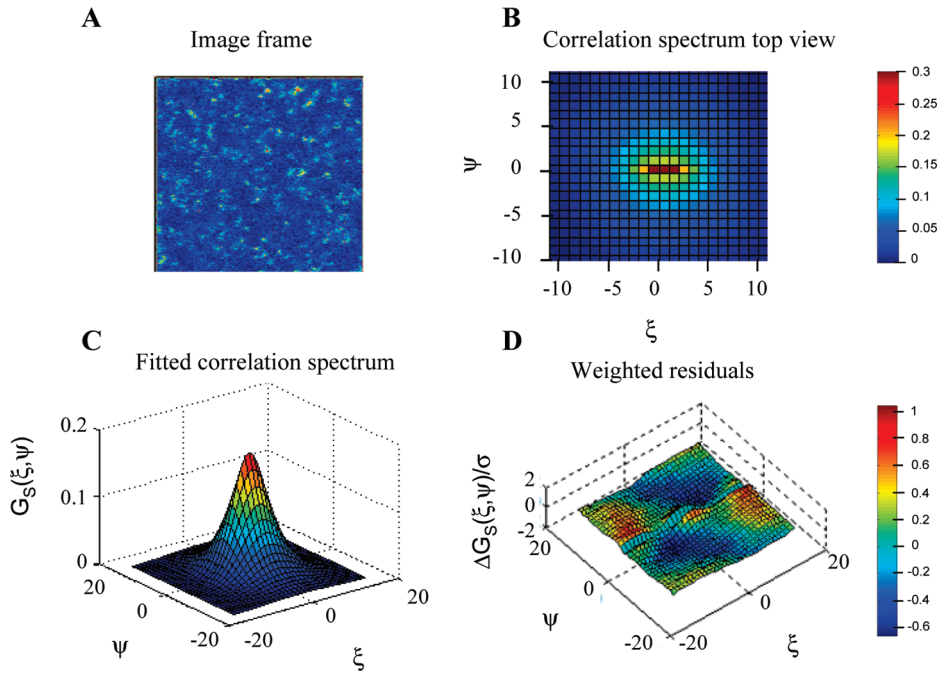

Figure 3. Subresolution fluorescent beads (175 nm diameter) freely diffusing in a 40% sucrose solution at 23 °C. Scales for the ξ and ψ axes in panels B, C, and D are in pixels. (A) Upper left quadrant of a 512 × 512 pixel raster-scan image; (B) top view of the measured correlation spectrum; (C) fitted correlation spectrum (3D free diffusion model); and (D) corresponding weighted residuals. Twenty images were collected at a scan speed of 9. Pixel size δr = 54.9 nm; τ_p = 1.6 μs; τ_l = 1.92 ms. Parameter values are summarized in Table 1. Color bar maps $G_S(\xi,\psi)$ values.

Table 1. 3D RICS Diffusion Measurements on 175 nm Beads in Isotropic Solution at 23 °C

solution	η (mPa·s)	τ_p (μs)	τ_l (ms)	D^a (μm^2/s)	$D_{expected}{}^b$ (μm^2/s)
HEPES (5% Tween 20)	0.93	0.8−12.8	0.96−15.36	2.4 ± 0.4	2.7
2% sucrose	0.96	0.57−25.6	0.68−30.72	2.9 ± 0.7	2.6
10% sucrose	1.09	0.91−51.2	1.09−61.44	2.4 ± 0.5	2.3
40% sucrose	1.95	0.8−102.4	0.96−122.88	1.4 ± 0.1	1.3
56% sucrose	3.33	0.57−6.4	0.68−7.68	0.7 ± 0.1	0.7

[a] Uncertainties are reported as standard errors. [b] Calculated according to the Stokes−Einstein equation.

similar diffusion coefficients are retrieved. Mapping of a larger 256 × 256 pixel GUV top area results in a systematic drop-off of the D values but only near the mapping perimeter, apparently because one starts observing diffusion in areas with curvature.

RICS Measurements on DiI-C_{18}(5) in Cell Membranes of Living OLGs. Raster-scan images were collected in 29 shake-off cells of three different batches. In each cell, one to four separate 32 × 32 and/or 64 × 64 ROIs were selected for data analysis. Selected areas were at a certain distance from cell rims and showed rather homogeneous fluorescence intensity. The corresponding autocorrelation spectra were cropped to 32 × 32 regions and fitted with a 2D diffusion model. The majority (i.e., 69%) of the analyzed ROIs yield a diffusion coefficient smaller than or equal to D = 4 μm^2/s (Figure 5). This was also the case when larger ROIs (i.e., 128 × 128 pixels) were analyzed (data not shown).

As mentioned earlier, one of the advantages of RICS is that kinetic information can be spatially mapped allowing for the detection of heterogeneities in diffusion. This mapping is demonstrated in Figure 6 for a single primary OLG. The uncertainty in the separate D values is about 10−30%.

FRAP Measurements on DiI-C_{18}(5) in Cell Membranes of Living OLGs. FRAP measurements performed on 10 individual primary OLGs labeled with DiI-C_{18}(5) yield D values (0.4 ± 0.2 μm^2/s ≤ D ≤ 2.8 ± 0.3 μm^2/s) that are within the same range as the majority of D values obtained via RICS (Figure 5). A typical FRAP curve obtained in shake-off OLGs is shown in Figure 7. The weighted mean of the mobile fraction M of DiI-C_{18}(5) was found to be M = 89.5 ± 0.5%.

Discussion

In this paper, we described the implementation and performance of RICS on a one-photon Zeiss LSM510 META CLSM with analog detection. The detector autocorrelation time imposes an upper limit onto the diffusion coefficient that can be measured. The determination of fast diffusion requires high scan speeds, leading to increased spatial correlation induced by the detector. The detector electronics does not have enough time to reset itself before collecting the next data point. As a result, the residual signal from the previous data point will be correlated with the signal from the following data point. It is important to eliminate these bleed-through noise data points before fitting the spatial ACF since they can result in a lack of convergence of the fitting functions.[16] For the diffusion coefficients considered here, it was possible to discard the spatial correlations along the x-axis (ψ = 0), allowing the recovery of diffusion times ranging up to several tens of squared micrometers per second. However, depending

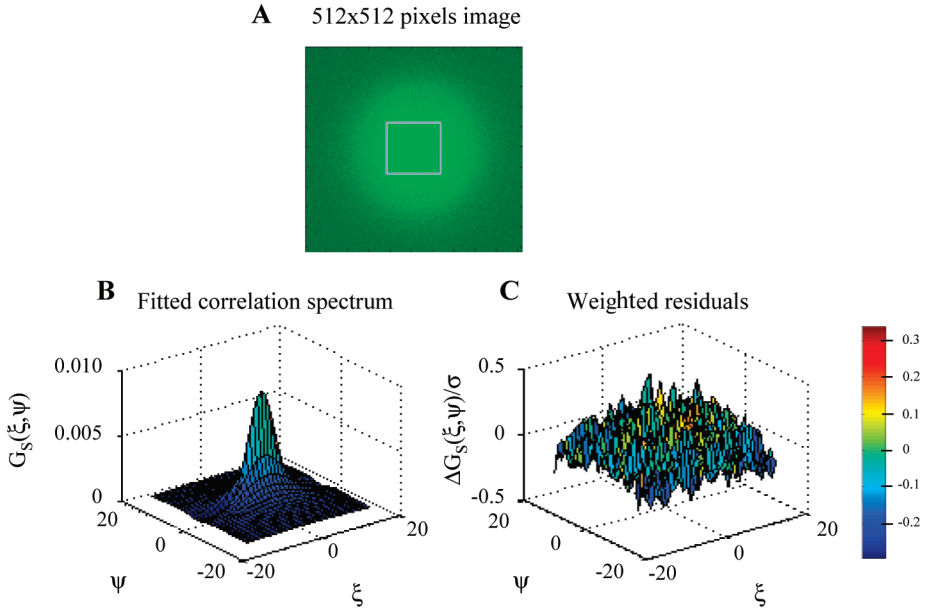

Figure 4. RICS data obtained from a single POPC/DiI-C_{18}(5) GUV. (A) Raster-scan image of the top membrane of the GUV. Scales for panels B and C are in pixels. The white bordered square reflects the 128 × 128 pixel ROI, which was selected for data analysis. (B) fitted correlation spectrum (2D free diffusion model) and (C) corresponding weighted residuals. 100 images were collected at a scan speed of 9. Pixel size δr = 54.9 nm; τ_p = 1.6 μs; τ_l = 1.92 ms; T = 22 °C. Color bar maps $G_S(\xi,\psi)$ values.

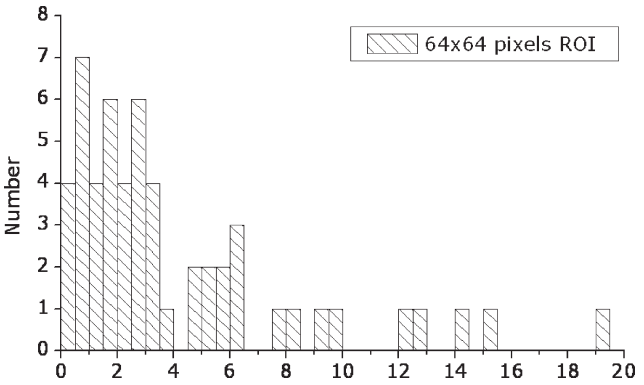

Figure 5. Histograms showing D values obtained from RICS measurements on DiI-C_{18}(5) in primary OLGs. Fifty-four 64 × 64 ROIs were selected for data analysis.

on the sample properties and the corresponding instrument settings, the dynamic range for our instrument would allow spatial correlations along the x-axis (ψ = 0) for long pixel dwell times τ_p = 163.84 and 102.4 μs (scanspeeds 1 and 2) and for gain settings below 1000.

The accuracy of the RICS approach to determine diffusion coefficients was assessed in isotropic viscous solutions of 175 nm fluorescent beads. Data were analyzed with both the UCI and UH RICS software. Both software programs yielded similar results, which were in good agreement with the Stokes−Einstein free translational diffusion model (Table 1), indicating that the RICS method and the in-house software for data analysis are compatible for well-characterized, chemically and optically homogeneous samples.

The applicability of RICS to monitor 2D diffusion was evaluated by performing measurements on the top membrane of POPC/DiI-C_{18}(5) GUVs, a model membrane system also characterized by means of beam expander FCS. FRAP measurements in GUVs showed that nearly all DiI-C_{18}(5) molecules (M = 97 ± 2%) are mobile. The mean D value (D = 7 ± 3 $\mu m^2/s$) obtained by RICS was in good agreement with the D values deduced from the beam expander FCS diffusion law fit (D_{eff} = 8.02 ± 0.01 $\mu m^2/s$). These values are also in good agreement with those reported in the literature for DiI-C_{18} in 1,2-dioleoyl-*sn*-glycero-3-phosphatidylcholine (DOPC) GUVs (D = 7.0 ± 1.2 $\mu m^2/s$).[34] FRAP measurements performed on DiI-C_{18} in POPC-supported phospholipid bilayers undergoing minimal interactions with the substrate yield a diffusion coefficient that is equal to the value we obtained via RICS in POPC GUVs (D = 7.5 ± 1.2 $\mu m^2/s$).[35] Consistent results were obtained for the mapped diffusion coefficient values for varying sizes of the analysis ROI as long as the GUV perimeter was avoided

RICS was applied to monitor the diffusion of DiI-C_{18}(5) in the membrane of primary OLGs derived from neonatal rat brain (i.e., shake-off cells). Measurements in cell membranes are obviously more challenging than those in homogeneous solutions or in fluid-phase model membrane systems. The images of cell membranes often exhibit large immobile structures, possibly cytosolic vesicles, which will appear as long-range spatial correlations in the autocorrelation spectrum and which may hide other potentially more meaningful information.[14,16] These immobile structures, however, were filtered out of the images by applying a moving average window of two frames before calculation of the autocorrelation spectra. Note that the relationship between $G(0,0)$ and the number of particles is no longer valid when the subtraction algorithm (overall or moving average) is applied and the $G(0,0)$ value can no longer be used as a direct measure of the molecular concentration.[14,16] Fitting the autocorrelation spectra calculated for DiI-C_{18}(5) in shake-off cells to a single free diffusing component gave diffusion coefficients (D = 0.12−4 $\mu m^2/s$) that compare well with the FRAP measurements performed here ($0.4 \pm 0.2\,\mu m^2/s \le D \le 2.8 \pm 0.3\,\mu m^2/s$) as well as D values reported for FCS (D = 3 ± 1 $\mu m^2/s$;[34]

(34) Bacia, K.; Scherfeld, D.; Kahya, N.; Schwille, P. *Biophys. J.* **2004**, *87*, 1034–1043.
(35) Orth, R. N.; Kameoka, J.; Zipfel, W. R.; Ilic, B.; Webb, W. W.; Clark, T. G.; Craighead, H. G. *Biophys. J.* **2003**, *85*, 3066–3073.

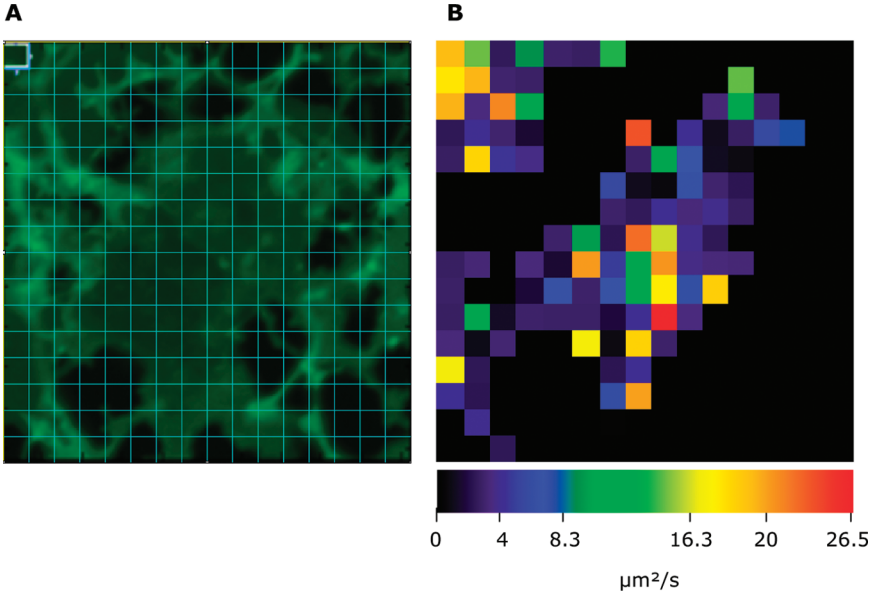

Figure 6. Spatial mapping of diffusion coefficients. (A) 512 × 512 pixel raster-scan image of a primary OLG labeled with DiI-C_{18}(5). The image is subdivided in 32 × 32 pixel ROIs (total area of 3.1 μm^2) for data analysis. Overlay grid pattern (light blue) outlines the ROI mapping. (B) Corresponding D map showing the spatial heterogeneity in the diffusion of DiI-C_{18}(5). D values vary between 0.4 and 26.5 $\mu m^2/s$, and are respectively dark blue and red in the lookup table. ROIs at the edge of the cell and ROIs only containing background were not analyzed (black areas in B). 100 images were collected at a scan speed of 9. Pixel size δr = 54.9 nm; τ_p = 1.6 μs/pixel; τ_l = 1.92 ms; T = 20 °C.

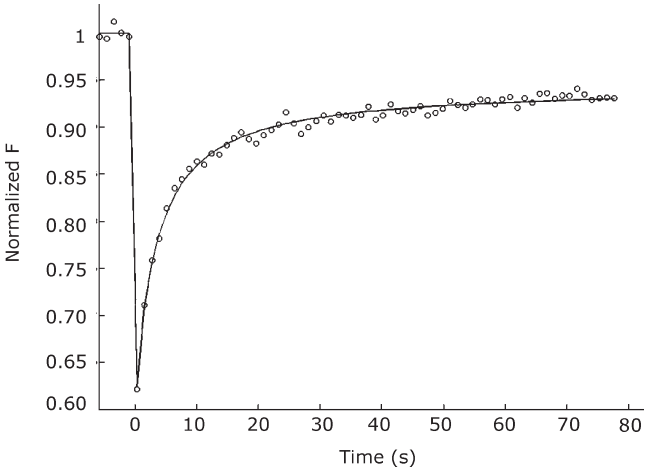

Figure 7. Typical FRAP curve obtained in shake-off OLGs labeled with DiI-C_{18}(5). A circular ROI of 160 pixels diameter (i.e., 8.784 μm) was selected in the bottom membrane of the cell underneath the nucleus. Seventy 512 × 512 pixel images were collected at a scan speed of 9 (i.e., 983.04 ms/frame) with a delay of 223 ms between two images: 5 before and 65 after the bleaching scan (a single bleach ROI scan at 80% of the AOTF maximum intensity, duration 307.2 ms). Open circles represent the experimental data. The solid line indicates the corresponding fit. D = 2.8 ± 0.3 $\mu m^2/s$, and M = 89.5 ± 0.5%.

D = 4.5 ± 0.8 $\mu m^2/s$[36]) and FRAP measurements (D = 1−4 $\mu m^2/s$[37,38]) on DiI-C_{18} in other cell membranes. However, comparison between FRAP and RICS results cannot directly be made, even when the ROI is of comparable size. In a FRAP experiment, the mobility of the fluorescent molecules in the nonbleached area is indirectly sampled as well. The value of D obtained in RICS is more locally defined. RICS is therefore more appropriate for detecting different molecular mobilities in spatially different areas of the cell membrane. This allows for mapping of the diffusion coefficient over the cell membrane, as shown in Figure 6 for DiI-C_{18}(5) in the membrane of shake-off OLGs. Note that ROIs near or crossing cell membranes were not analyzed.[14] On the other hand, since the current implementation of RICS does not allow for determination of immobile fractions, FRAP measurements are useful to quantify the mobile fraction of the molecules under study.

Interpretation of the mapped diffusion coefficients over the cell membrane is not obvious at this very moment. As has been observed, processes of neighboring cells that extend under the cell areas might be simultaneously imaged. However, by selecting areas that upon visual inspection show a homogeneous fluorescence intensity, diffusion coefficient values are found that correspond with those obtained for DiI-C_{18}(5) using FRAP. Higher diffusion coefficient values seem to be often associated with areas where bright spots near or inside cell processes or near the perimeter of the cell are present. Further exploration is obviously required and might imply drug-induced modification of intracellular structures.

In order to accurately calculate and fit the autocorrelation spectrum, it is important to collect a sufficient number of images. Note that the number of frames is tightly connected to the size of the analysis ROI. For smaller ROIs, more frames are needed, thereby increasing spatial resolution at the expense of temporal resolution, and vice versa. An alternative way to reduce the exposure of cells to laser light is by keeping the laser power low, which usually involves a high detector gain, possibly resulting in noisy images. This thermal noise due to the high detector gain, however, is truly random and will not contribute to the autocorrelation spectrum.[16] Immobile or slowly moving subcellular structures, on the other hand, do strongly influence the spatial correlations. When measuring in living motile OLG cells, it is therefore imperative to subtract these features by applying a moving average

(36) Humpolíčková, J.; Gielen, E.; Benda, A.; Fagulová, V.; Vercammen, J.; vandeVen, M.; Hof, M.; Ameloot, M.; Engelborghs, Y. *Biophys. J.* **2006**, *91*, L23–L25.
(37) Fulbright, R. M.; Axelrod, D.; Dunham, W. R.; Marcelo, C. L. *Exp. Cell. Res.* **1997**, *233*, 128–134.
(38) Weisswange, I.; Bretschneider, T.; Anderson, K. I. *J. Cell. Sci.* **2005**, *118*, 4375–4380.

immobile fraction removal algorithm before calculating autocorrelation spectra.

The acquisition of fewer frames requires less collection time, allowing one to observe cellular changes on a shorter time scale. However, this is at the expense of the quality of the collected data.

Conclusions

It is shown in this paper that RICS can be performed on a Zeiss LSM510 META laser-scanning confocal system with one-photon excitation and analog detection. The unwanted correlations introduced by the detection system have to be characterized and effectively removed before fitting the spatial correlation spectra. For the considered Zeiss LSM510 META (build 2002) system and our sample properties, this implied that, for most scan parameter settings, the $\psi = 0$ line had to be removed so that the dynamic range was essentially determined by the line time. If possible, however, it is much better to avoid this complication altogether and to work with photon counting detection.[16] Nevertheless, RICS with analog detection exhibits a sufficiently large dynamic range to study the diffusion of both lipid analogs and membrane proteins.

The RICS approach provides a valuable means to map the local variation in diffusion coefficients over model and cell membranes. The values for the diffusion coefficients are comparable with those obtained by FRAP and FCS. However, as compared to FRAP, RICS imposes less power on the sample and allows for more locally defined diffusion coefficients. As compared to FCS, RICS covers a much wider area. Similarly to FRAP and FCS, curvature effects have to be avoided by selecting an appropriate analysis ROI size. The influence of curvature in model membranes can be retrieved by mapping with various size analysis ROIs. Observation of model and cell membranes over smaller areas increases spatial resolution but results in smaller ROIs with a smaller total number of observation pixels, thus requiring more frames to maintain an appropriate signal-to-noise ratio.

Acknowledgment. We sincerely thank Prof. P. Wiseman and Dr. D. Kolin, McGill University, Montreal, Canada, for providing free access to core Matlab routines and for helpful discussions, Dr. N. Kahya (Philips, Eindhoven) and Dr. A. Margineanu (Imperial College London) for useful advice towards the preparation of the GUVs, Dr. K. Weisshart and Dr. M. Marx, Zeiss, Jena, Germany, and Mr. D. Van Meensel of Zeiss NV/SA Belgium for elucidating scan parameter values, and Mrs. H. Penxten for performing viscosity measurements. This work was funded by the Research Council of the UHasselt, tUL, the K.U.Leuven (GOA/2006/02) and by a Ph.D. grant of the Institute for the Promotion of Innovation through Science and Technology in Flanders (IWT-Vlaanderen). Support by IAP P6/27 Functional Supramolecular Systems (BELSPO) and by the FWO-onderzoeksgemeenschap "Scanning and Wide Field Microscopy of (Bio)-organic Systems" is gratefully acknowledged.